PCCP

PAPER

View Article Online
View Journal | View Issue

Cite this: *Phys. Chem. Chem. Phys.*, 2015, **17**, 20134

The *cis*-isomer performs better than the *trans*-isomer in porphyrin-sensitized solar cells: interfacial electron transport and charge recombination investigations

Liyang Luo,*[a] Ram B. Ambre,[a] Sandeep B. Mane,[a] Eric Wei-Guang Diau*[b] and Chen-Hsiung Hung*[a]

Received 23rd April 2015,
Accepted 29th June 2015

DOI: 10.1039/c5cp02367j

www.rsc.org/pccp

We report characterizations and device performance for dye-sensitized solar cells using *cis*- and *trans*-isomers of 2D–π–2A zinc porphyrins with carboxyphenyl and thienyl groups in their *meso*-positions. Under identical experimental conditions with similar dye loadings, we observed overall power conversion efficiencies of 2.44% and 0.88% for devices made of *cis*-2S2A and *trans*-2S2A, respectively. This uneven performance among *cis* and *trans* isomers under the same experimental conditions can be rationalized with detailed investigations *via* spectroscopic, quantum chemical, and femtosecond fluorescence up-conversion investigations. Density functional theory (DFT) calculations show that a small amount of electron density is localized over carboxyphenyl groups in the LUMO of *cis*-2S2A, but there is no electron density populated on the carboxyphenyl groups in the LUMO of *trans*-2S2A. The femtosecond fluorescence decay measurements revealed that the excited-state lifetime of *trans*-2S2A on Al_2O_3 is half of that of *cis*-2S2A on Al_2O_3. Moreover, the dye-to-TiO_2 electron injection time of *trans*-2S2A is 2.54 ps, which is shorter than that of *cis*-2S2A/TiO_2 (2.95 ps). Electrochemical impedance spectra measured under one sun illumination also revealed that the charge recombination time of *cis*-2S2A is longer than that of *trans*-2S2A. This thorough understanding of isomeric effects on the performance of porphyrins will serve as a guideline for the design of future sensitizing dyes for solar cells.

Introduction

Global warming has already had observable effects on our climate, community, and health. Hence, researchers worldwide are pursuing the ideas of harnessing renewable energy options to reduce our dependence on fossil fuels.[1,2] One of these renewable energy alternatives is the use of photovoltaic cells to convert solar energy into electrical energy. Among the various photovoltaic cells, recently investigated new generation solar cells known as dye-sensitized solar cells (DSSCs) composed of sensitizing dye, electrolyte, and electrodes have attracted tremendous attention.[3–5] The key component of the DSSC is the photosensitizing molecule, which absorbs solar radiation and converts it into electrical energy. Porphyrins are optimal sensitizers in DSSCs due to their strong absorption in the *Soret* band region and moderate absorption in the Q band region. In addition, the HOMO–LUMO energy levels of zinc porphyrins match well with the requirements for dye-sensitized solar cells.[6–8] Moreover, it is revealed from photophysical measurements that the kinetics of electron injection from zinc porphyrins into the conduction band of TiO_2 is indistinguishable from the reported highest efficiency ruthenium sensitizers.[9] Recently, Lin and co-workers reported several zinc porphyrins with 10% efficiency, based on a push–pull type D–π–A system.[10–13] A major breakthrough for the utilization of zinc porphyrin dyes was the push–pull zinc porphyrin sensitizer YD2 with a diarylamino electron-donating group and an ethynylbenzoic acid moiety serving as the electron-acceptor, which demonstrated an η value of 11% under standard illumination conditions.[14] The porphyrin sensitizer YD2-*o*-C8 of a similar framework has demonstrated 12% efficiency under standard one sun illumination conditions combined with a cobalt electrolyte.[15] The record high efficiencies of 12.75% and 13% have been achieved by D–π–A type porphyrin dyes, GY50 and SM315, respectively, when assembled with a cobalt electrolyte under standard one sun illumination.[16,17] Majority of the DSSC research is focused on 1D–π–1A type porphyrins. Although it has been observed that the position and type of anchoring groups of the dye play important roles in determining the

[a] *Institute of Chemistry, Academia Sinica, Taipei-115, Taiwan, Republic of China. E-mail: chhung@gate.sinica.edu.tw*
[b] *Department of Applied Chemistry and Institute of Molecular Science, National Chiao-Tung University, Hsinchu-30010, Taiwan, Republic of China. E-mail: diau@mail.nctu.edu.tw*

performance and stability of the device, very few examples of multi donor–acceptor porphyrins to study the orientation effects on the photovoltaic performance have been reported in literature.[18,19] There are only a handful of reports in the literature using *cis*-/*trans*-isomers of zinc porphyrins as the sensitizer in DSSCs;[20–26] however, detailed investigations comparing porphyrin orientations with their photovoltaic performance are still necessary. The excited-state relaxation dynamics and the interfacial charge transfer mechanisms for these *cis*-/*trans*- isomers will help understand the orientation effects of donor/acceptor groups on the DSSC performance.

Our group has been involved in the development of multi-anchor porphyrins,[27–31] core-modified[32,33] and expanded porphyrins[34,35] for application as sensitizers in DSSCs. Our prior systematic studies of a series of *meso*-thienyl and carboxyphenyl substituted zinc porphyrins, namely, 3S1A, *trans*-2S2A, *cis*-2S2A, and 1S3A, elucidated significant influence of position and number of carboxyphenyl and thienyl groups on the electrochemical and photovoltaic properties. We systematically studied the effects of carboxyphenyl as an anchoring group and the heavy atom effect of thiophene in zinc porphyrins on the power conversion efficiency. During these studies, we observed for the first time that devices made of structural isomers *cis*-2S2A and *trans*-2S2A (Scheme 1) under the same experimental conditions showed distinctly different photovoltaic performance. We carried out quantum chemical calculations, femtosecond fluorescence up-conversion and electrochemical impedance spectroscopy measurements in order to understand the correlations between the isomeric structure and device performance for *cis*-2S2A and *trans*-2S2A porphyrins applied in DSSCs.

Experimental section

1. Synthesis

The synthetic details and characterization data of *cis*-2S2A and *trans*-2S2A have been reported elsewhere.[27]

2. Characterization

The absorption spectra of the porphyrins in THF were obtained using a JASCO V-670 UV-Vis/NIR spectrophotometer. Steady-state fluorescence spectra were acquired using a Varian Cary Eclipse fluorescence spectrophotometer. The density functional theory (DFT) and time-dependent density functional (TD-DFT) calculations were performed with the GAUSSIAN 09 package to study the electron distribution of the frontier molecular orbitals and the photoexcitation transitions.[36] All ground state geometries of the porphyrins studied were optimized in the gas phase by the hybrid B3LYP functional and the 6-31G basis set. The TD-DFT calculations were based on the same functional and basis set. The molecular orbitals were visualized by the ChemOffice software Chem 3D Ultra 2013.

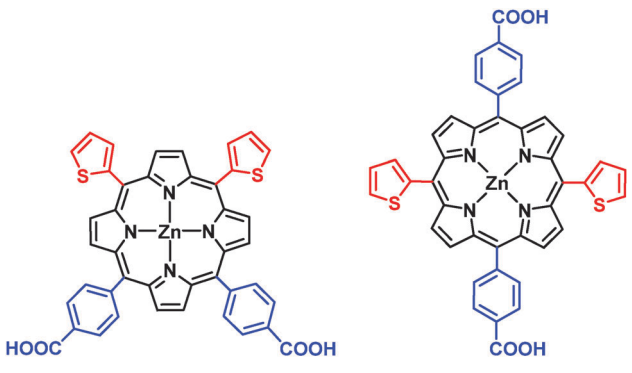

cis-2S2A *trans*-2S2A

Scheme 1 Molecular structures of *cis*-2S2A and *trans*-2S2A.

3. Photovoltaic measurements

To characterize the photovoltaic performance of the DSSC devices, a fluorine-doped tin oxide (FTO; 30 Ω sq^{-1}, Sinonar, Taiwan) glass (typical size 1.0 × 2.0 cm) coated with platinum nano-cluster catalyst using the thermal decomposition method was used as the cathode.[37] The Pt catalyst was coated using a precursor solution composed of 5 mM solution of hexachloroplatinic acid in anhydrous isopropanol through spin-coating on the FTO glass and dried in air for 3 min. The Pt electrode was gradually heated in an oven at 360 °C for 15 min. The TiO_2/porphyrin layer served as the working electrode (anode). We immersed the TiO_2 coated FTO[38,39] (TiO_2 thickness 7 ± 0.5 μm, active area 0.4 × 0.4 cm^2) in a THF solution containing *trans*-2S2A (1 × 10^{-4} M) and *cis*-2S2A (2 × 10^{-4} M) at 40 °C for 3 h. To fabricate the DSSC device, the two electrodes were assembled into a sandwich type cell, spaced, and sealed with a hot-melt film (SX1170, Solaronix, thickness 30 μm). The thin layer of electrolyte was introduced into the space between the two electrodes.[40] A typical redox electrolyte contained 50 mM iodine (I_2), 0.5 M lithium iodide (LiI), 0.6 M 4-*tert*-butylpyridine (TBP), and 0.5 M dimethyl-propyl-benzimidiazole iodide (DMPII) in dry acetonitrile. Under similar conditions, the average efficiency of N719 is 7% and the fill factor is 0.71. The photocurrent and voltage curves were recorded with a digital source meter (Keithley 2400) under AM 1.5 one sun irradiation (100 mW cm^{-2}, AM 1.5 G) from a solar simulator (Sanei Electric XES-502S) calibrated with a Si-based reference cell (Hamamatsu S1133). The IPCE measurements were carried out with a homebuilt system, which includes a Xe lamp (PTi A-1010, 150 W), a monochromator (Dongwoo DM150i, 1200 g mm^{-1} blazed at 500 nm), and a source meter (Keithley 2400). A standard Si photodiode (ThorLabs FDS1010) was used as a reference to calibrate the power density of the light source at each wavelength so that the IPCE of the DSSC device could be obtained.

4. Femtosecond lifetime measurements

The dynamics of excited states of zinc porphyrins on TiO_2 were measured with the fluorescence up-conversion technique. Basically, a fluorescence optically-gated (up-conversion) system (FOG100, CDP) is implemented in combination with a mode-locked Ti-sapphire laser (Mira 900D, Coherent) pumped with a 10 W Nd:YVO4 laser (Verdi-V10, Coherent). The femtosecond laser system generates output pulses at 860 nm (or 840 nm) with duration of 120 fs at a repetition rate of 76 MHz. The frequency of the laser pulse was doubled for excitation. The residual fundamental

pulse was used as an optical gate; a dichromic beam splitter was used to separate excitation and gate beams. The excitation beam intensity was appropriately attenuated, and then focused onto a 1 mm rotating cell containing either the solution or the solid thin-film samples. The femtosecond system includes two optical paths for excitation: path one is designed for measurements of thin-film samples *via* collection of emission from the front face, while the second path is designed for measurements of solution samples *via* collection of emission from the back face. The emission was collected with two parabolic mirrors and focused onto a crystal (BBO type-I); the gate pulse was also focused onto that BBO crystal for sum-frequency generation. The latter signal was collected with a lens and separated from interference light with an iris, a band-pass filter, and a double monochromator (DH10, Jobin Yvon) in combination, then detected with a photomultiplier (R1527P, Hamamatsu) connected to a computer-controlled photon-counting system. On varying the temporal delay between gate and excitation pulses *via* a stepping-motor translational stage, we obtained a temporal profile (transient). The polarization between pump and probe pulses was fixed at the magic angle conditions. The fluorescence transient signals were fitted through convolution of the instrument-response function with the molecular response function containing multi-exponential decay components.[41]

Results and discussion

Absorption spectra

The absorption coefficients and fluorescence intensities of *cis*-2S2A and *trans*-2S2A were measured in THF. Although structural conformations of *cis*-2S2A and *trans*-2S2A are different, Fig. 1 shows similar optical absorption wavelengths for both isomers in THF solution. The intense *Soret* peak is at 427 nm, and the Q(1, 0) and Q(0, 0) peaks are at 558 and 600 nm, respectively, and the extinction coefficient at the *Soret* peak is about twenty times more intense than that of the Q(1, 0) peak in both *trans*-2S2A and *cis*-2S2A.

The extinction coefficient of *trans*-2S2A is higher than that of *cis*-2S2A, which means that the radiative lifetime of *trans*-2S2A is shorter compared to that of *cis*-2S2A. The fluorescence spectra of *cis*-2S2A and *trans*-2S2A were measured in THF by exciting at the *Soret* band wavelength. The fluorescence spectra of both zinc porphyrins display the same emission maxima of Q(0, 0) and Q(0, 1) bands, indicating that the fluorescence is dominantly emitted at the S_1 state and the excited lifetimes for both the isomers are similar, about 1.5 ns under air. Previous investigations by our group showed that the excited state lifetime is strongly dependent on the number of thienyl groups at the *meso*-position controlled by the presence of a heavy atom effect. However, *cis*-2S2A and *trans*-2S2A have the same number of thienyl groups, thus allowing us to examine the orientation effect of *cis*-2S2A and *trans*-2S2A under an identical heavy atom effect.

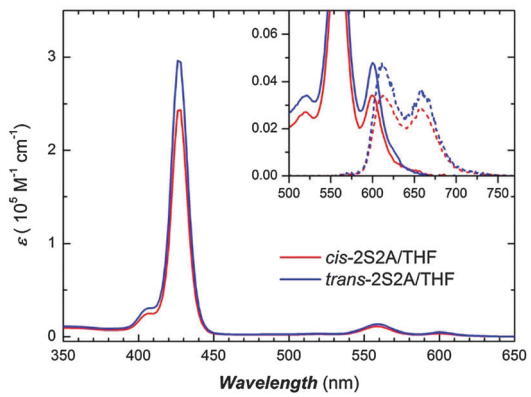

Fig. 1 Absorption spectra of *cis*-2S2A and *trans*-2S2A in THF. Inset shows absorption and fluorescence spectra with the intensity of fluorescence spectra normalized with the absorption peaks of the Q(0, 0) bands.

DFT and TD-DFT calculations

The molecular orbitals of *cis*-2S2A and *trans*-2S2A at various energy levels are shown in Fig. 2. The distributions of electron density in HOMO, LUMO, and LUMO+1 of *cis*-2S2A and *trans*-2S2A are mainly localized on the π orbitals of the conjugated porphyrin ring. For HOMO orbitals, some π electron density distributes onto thienyl groups of both *cis*-2S2A and *trans*-2S2A. In the LUMO and LUMO+1 of *cis*-2S2A, it is observed that a part of the π electron density is localized over one of the two carboxyphenyl groups; whereas, for *trans*-2S2A, there is no π electron density localized on any carboxyphenyl in the LUMO; and in the LUMO+1 of *trans*-2S2A, the electron density is located on both of the carboxyphenyl groups. This indicates that electron injections from the LUMO and LUMO+1 levels into the conduction band of TiO_2 are feasible in *cis*-2S2A, while the excited electrons in *trans*-2S2A are unlikely to inject from the LUMO level into the conduction band of TiO_2. As interpreted in Fig. 3 for both isomeric porphyrins, electron injections may occur from both LUMO and LUMO+1 levels for *cis*-2S2A but it is feasible only from the LUMO+1 level for *trans*-2S2A. This may be one of the reasons that accounts for the lower efficiency of the *trans*-2S2A device than the *cis*-2S2A device, for which the details will be given in the next section. Moreover, the π electrons in the two LUMO+2 levels are dominantly distributed over the carboxyphenyl groups. The electronic injections involving the LUMO+2 level may be more efficient for *cis*-2S2A than for *trans*-2S2A due to a dual anchoring mode.

The excitation energies (E) and oscillation strengths (f) of the first four singlet electronic transitions (S1–S4) of *cis*-2S2A and *trans*-2S2A were obtained *via* the TD-DFT calculations; the corresponding results are shown in Table 1. For *cis*-2S2A and *trans*-2S2A, the four singlet electronic transitions are similar. The major compositions of these electronic transitions include HOMO−1, HOMO, LUMO, and LUMO+1, and minor compositions of S3 and S4 electronic transitions include LUMO+2 and LUMO+3. The LUMO+2 and LUMO+3 show that higher π electron density localized on both carboxyphenyl groups in the S3 and S4 electronic transitions of *cis*-2S2A and *trans*-2S2A might cause efficient charge separation and increase electron injection rate.

We also carried out Mullikan charge analysis for these isomeric porphyrins to understand the reasons behind the

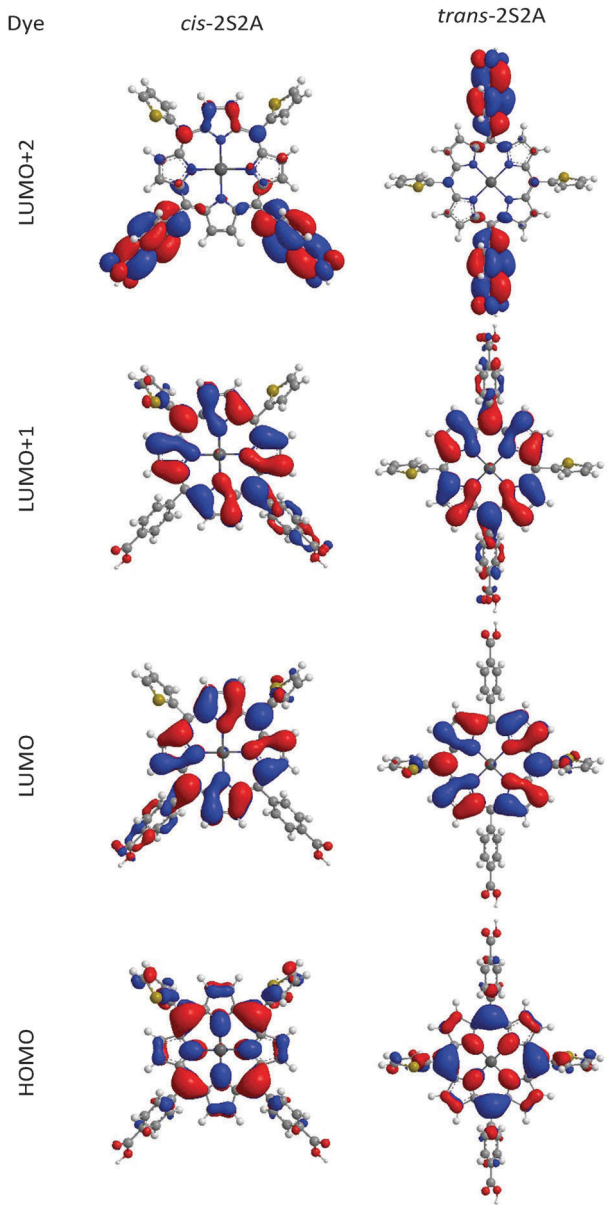

Fig. 2 Frontier molecular orbitals of *cis*-2S2A and *trans*-2S2A calculated at the B3LYP/6-31G level of theory.

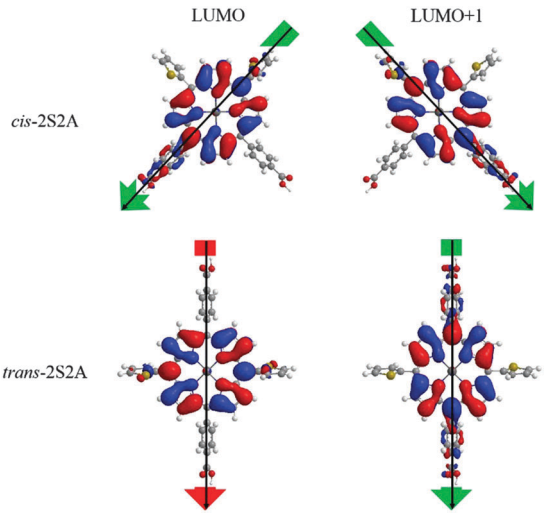

Fig. 3 Different electron density distribution in the LUMO and LUMO+1 orbitals for *cis*-2S2A and *trans*-2S2A.

Table 1 Calculated TD-DFT composition in terms of molecular orbitals, excitation energy, and the oscillator strengths of *cis*-2S2A and *trans*-2S2A[a]

Dye	State	Composition	(%)	E (eV), (nm)	f
cis-2S2A	S1	H−1 → L+1	42	2.299, 539.3	0.0119
		H → L	55		
	S2	H−1 → L	43	2.301, 538.9	0.0101
		H → L+1	54		
	S3	H−1 → L+1	42	3.174, 390.7	1.0461
		H → L	32		
		H → L+2	5		
	S4	H−1 → L	42	3.184, 389.4	1.1.77
		H → L+1	34		
		H → L+3	4		
trans-2S2A	S1	H−1 → L+1	42	2.295, 540.3	0.0163
		H → L	58		
	S2	H−1 → L	46	2.299, 539.4	0.0072
		H → L+1	54		
	S3	H−1 → L	40	3.160, 392.4	1.2347
		H → L+1	34		
		H → L+3	8		
	S4	H−1 → L+1	36	3.178, 390.1	0.8800
		H → L	25		
		H−1 → L+3	2		

[a] H = HOMO, L = LUMO, H−1 = HOMO−1, L+1 = LUMO+1, L+2 = LUMO+2, and L+3 = LUMO+3.

superior performance of *cis*-2S2A over *trans*-2S2A. We calculated the amount of electron density located on the carboxyphenyl anchor (CA) and the rest of the porphyrin (P) in the HOMO and LUMO and summarize them in Fig. 4. The electron density localized on CA in the LUMO of *cis*-2S2A is much higher than that in *trans*-2S2A, indicating that the charge injection probability might be higher in *cis*-2S2A than in *trans*-2S2A.

Photovoltaic characterizations

The current–voltage (J–V) characteristics were examined with the devices made with *cis*-2S2A and *trans*-2S2A sensitized on TiO_2 in the absence of CDCA. All samples were measured under identical and controlled molecular loading conditions. To adjust to near identical absorbances for both dyes adsorbed on metal oxide (TiO_2 and Al_2O_3) films, the concentration of *cis*-2S2A solution (1×10^{-4} M) was half of that of *trans*-2S2A (2×10^{-4} M). The J–V curves of the two devices are shown in Fig. 5; the corresponding photovoltaic parameters are summarized in Table 2.

As shown in Table 2, both J_{SC} and V_{OC} values are higher for the *cis*-2S2A device than for the *trans*-2S2A device. The dark J–V curves for *cis*-2S2A and *trans*-2S2A (Fig. 5b) are the same. In the case of *trans*-2S2A, which binds to the TiO_2 surface with only one anchoring unit, the distance between the triiodide and surface of TiO_2 is greater. On the other hand, the distance for back electron transfer for *cis*-2S2A could be shorter due to the

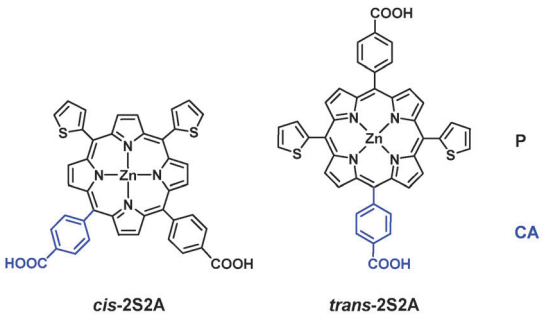

Dye	*cis*-2S2A		*trans*-2S2A	
	P	CA	P	CA
HOMO	99.02	0.98	99.12	0.88
LUMO	97.64	2.36	99.54	0.46
LUMO+1	97.81	2.19	97.68	2.32

Fig. 4 Mullikan charge analysis data for the studied porphyrins.

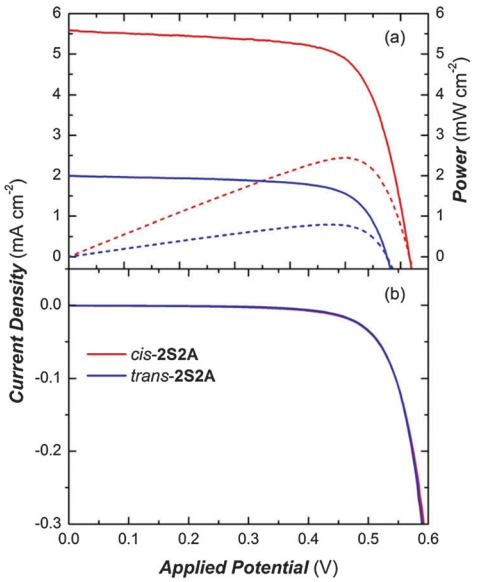

Fig. 5 *J*–*V* characteristics of *cis*-2S2A and *trans*-2S2A without CDCA (a) under AM 1.5 illumination and (b) under dark conditions.

Table 2 Photovoltaic performance of *cis*-2S2A and *trans*-2S2A

Dye	J_{SC} (mA cm^{-2})	V_{OC} (V)	FF (%)	η (%)
cis-2S2A	5.59	0.615	71	2.44
trans-2S2A	2.00	0.575	69	0.80

dual anchor bonding mode on TiO_2. Although the length of *trans*-2S2A adsorbed on TiO_2 is longer than that of *cis*-2S2A, the net shielding effect is similar for both porphyrins, as it is compensated for by the fact that the outer thienyl groups of *cis*-2S2A have more negative charge on the sulfur atom to repel I_3^- and therefore decrease the back electron transfer. Overall, although the position of the anchoring groups in *cis*-2S2A and *trans*-2S2A alters the photovoltaic performance, it does not change the dark current density under similar dye-loadings.

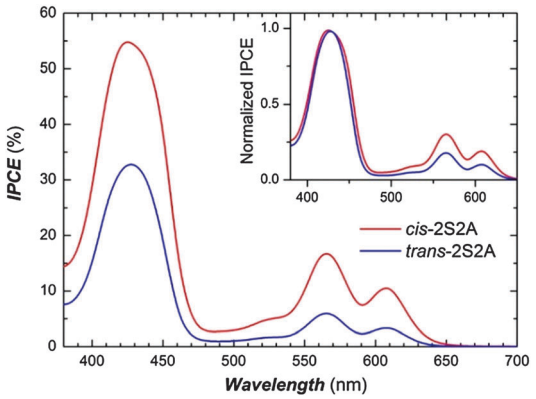

Fig. 6 IPCE spectra for dye-sensitized solar cells constructed with *cis*-2S2A and *trans*-2S2A without CDCA. The inset has the normalized IPCE spectra at the *Soret* peak.

In order to realize the current density at short-circuit, we measured the IPCE action spectra of the *cis*-2S2A and *trans*-2S2A devices under similar dye loadings; the results are shown in Fig. 6. From the IPCE spectra, we noticed that the quantum efficiency of photon-induced electron transfer at the *Soret* band is more effective than at the Q band. The IPCE values of all excitation wavelengths are significantly greater for *cis*-2S2A than for *trans*-2S2A. The efficiency of photo-current generation is dependent on three components: the light harvesting efficiency (LHE), electron injection efficiency (ϕ_{inj}) and charge collection efficiency (η_{cc}). The IPCE value at each wavelength is given by the product of the three efficiencies as:

$$\mathrm{IPCE}(\lambda) = \mathrm{LHE}(\lambda) \times \phi_{inj}(\lambda) \times \eta_{cc}(\lambda)$$

Under similar dye loadings on TiO_2 films confirmed by the absorption spectra of *cis*-2S2A and *trans*-2S2A, the major factors to determine the IPCE values of *cis*-2S2A and *trans*-2S2A should be ϕ_{inj} and η_{cc}. Therefore, we conclude that the product $\phi_{inj} \times \eta_{cc}$ is higher for *cis*-2S2A than for *trans*-2S2A. Moreover, both samples showed three times higher photocurrent density under short-circuit at the *Soret* band than at the Q bands. This result is attributed to better overlapping between the LUMO+2 and LUMO+3 orbitals of the porphyrins and the CB of TiO_2 when both molecules were excited at the wavelengths of the *Soret* band. The inset of Fig. 6 shows that the IPCE at the Q band region for *cis*-2S2A is greater than for *trans*-2S2A. The higher IPCE of *cis*-2S2A could be due to either the dual anchoring groups, which could increase the interfacial electron transfer process or the non-bonding anchoring group of *trans*-2S2A, which could decrease the efficiency of the electron injection process.

Femtosecond fluorescence decay measurements

Femtosecond fluorescence transients of *cis*-2S2A and *trans*-2S2A on Al_2O_3 and TiO_2 films are displayed in Fig. 7 and 8, respectively, with the excitation at 430 nm and the probe at 610 nm. The band edge of the conduction band of Al_2O_3 is higher than the S_2 and S_1 states of zinc porphyrins, which prohibits the interfacial electron transfer from the excited porphyrins to Al_2O_3.

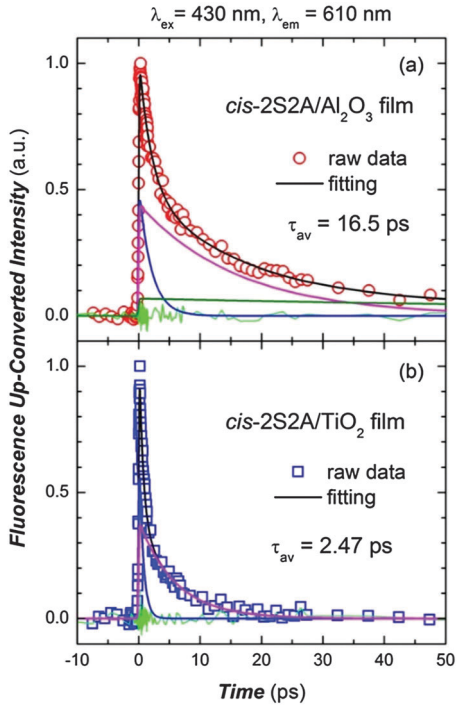

Fig. 7 Femtosecond fluorescence transients of *cis*-2S2A on (a) Al_2O_3 and (b) TiO_2 films with excitation at 430 nm and measured at 610 nm. Red circles and blue squares are raw data, black curves are fitting curves with multi-exponential function, green curves are residual analysis, and other colour curves are deconvoluted components.

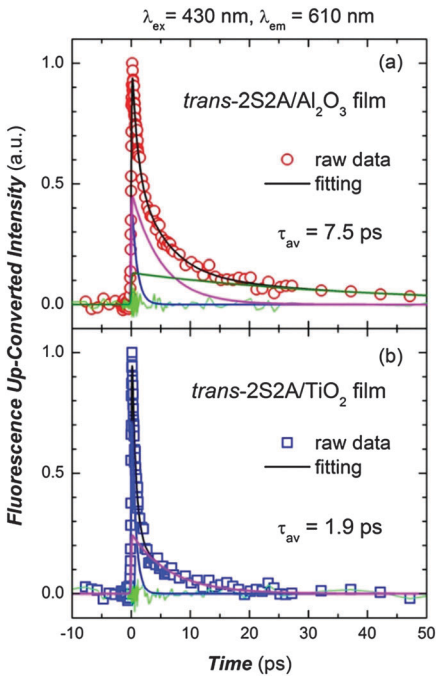

Fig. 8 Femtosecond fluorescence transients of *trans*-2S2A on (a) Al_2O_3 and (b) TiO_2 films with excitation at 430 nm and measured at 610 nm. Red circles and blue squares are raw data, black curves are fitting curves with multi-exponential function, green curves are residual analysis, and other colour curves are deconvoluted components.

Thus, the measurements of zinc porphyrins on Al_2O_3 film simply reflect the excited-state relaxation dynamics of the porphyrin itself. On the other hand, the fluorescence transient of zinc porphyrins on TiO_2 involves not only the excited-state relaxation process but also the interfacial electron transfer from the excited porphyrin to the conduction band of TiO_2. In order to obtain the yields of the electron injection, we measured the fluorescence decay times for both *cis*-2S2A and *trans*-2S2A porphyrins adsorbed on Al_2O_3 ($\tau_{Al_2O_3}$) and TiO_2 (τ_{TiO_2}) films. All fluorescence transients were fitted by an appropriate kinetic model with multi-exponential decay functions. The average fluorescence decay lifetime of a zinc porphyrin on Al_2O_3 film ($\tau_{Al_2O_3}$) can be dominated by the excited-state relaxation and an intermolecular aggregation quenching effect, while the average fluorescence decay lifetime of zinc porphyrin on TiO_2 film (τ_{TiO_2}) involves additional relaxation due to the interfacial electron transfer. From these two time coefficients, the time of interfacial electron injection (τ_{inj}) and the quantum yield of interfacial electron injection (ϕ_{inj}) can be expressed as[42]

$$\tau_{inj} = \frac{\tau_{TiO_2}\tau_{Al_2O_3}}{\tau_{Al_2O_3} - \tau_{TiO_2}} \quad (1)$$

$$\phi_{inj} = \frac{\tau_{TiO_2}}{\tau_{inj}} = \frac{\tau_{Al_2O_3} - \tau_{TiO_2}}{\tau_{Al_2O_3}} \quad (2)$$

The obtained interfacial electron injection times and quantum yields of *cis*-2S2A and *trans*-2S2A are listed in Table 3. According to the results obtained from the femtosecond fluorescence decay measurements, the electron injection rates of both *cis*-2S2A and *trans*-2S2A are comparable. The factor influencing the yield of interfacial electron transfer will be the excited-state relaxation of zinc porphyrins on the nanoparticles of Al_2O_3 or TiO_2.

Although the excited-state lifetimes for *cis*-2S2A and *trans*-2S2A in THF are similar (1.5 ns), the excited-state lifetime of *trans*-2S2A on Al_2O_3 film is one half that of *cis*-2S2A. The shorter excited-state lifetime can be ascribed to the effective aggregation quenching among *trans*-2S2A molecules on Al_2O_3. The effective intermolecular aggregation quenching of *trans*-2S2A on nanoparticle colloid surfaces could be mainly attributed to a shorter intermolecular distance for *trans*-2S2A than for *cis*-2S2A, because *trans*-2S2A molecule has a free non-bonding carboxyl group, which can induce intermolecular hydrogen bonding on the surface.

Electrochemical impedance spectroscopy (EIS) measurements under one sun condition

In general, V_{OC} is determined by the potential difference between the quasi Fermi level of TiO_2 and the HOMO level of

Table 3 Time coefficients of zinc porphyrins on Al_2O_3 and TiO_2 films, and interfacial electron injection times and efficiencies for *cis*-2S2A and *trans*-2S2A

Dye	$\tau_{Al_2O_3}$ (ps)	τ_{TiO_2} (ps)	τ_{inj} (ps)	ϕ_{inj} (%)
cis-2S2A	16.5	2.5	2.95	85
trans-2S2A	7.5	1.9	2.54	75

redox couples (E_{redox}) in the electrolyte, which could be described by the following equation:[43,44]

$$V_{OC} = \frac{E_{CB}}{q} + \gamma\frac{kT}{q}\ln\left(\frac{N_{CB}}{n}\right) - \frac{E_{redox}}{q}$$

where γ is a characteristic constant of the TiO_2 tailing states, k is the Boltzmann constant, T is the temperature, q is the elementary charge, and N_{CB} is the effective electron density of the states at the TiO_2 conduction band edge. In the same electrolyte, the V_{OC} of a zinc porphyrin sensitized solar cell is dependent on the quasi Fermi level of TiO_2 under the same E_{redox}. In addition, the number of electrons in the TiO_2 conduction band is determined by the balance between electron injection and charge recombination, which influences the quasi Fermi level in TiO_2. The higher V_{OC} of *cis*-2S2A than *trans*-2S2A is attributed to the larger number of electrons with high effective interfacial electron injection yield. However, not only the interfacial electron transfer yield, but also the rate of charge recombination between electrons in TiO_2 and redox couples in electrolyte can affect the V_{OC}. Therefore, the value of V_{OC} is closely related to the surface charge and charge recombination. As a consequence, the influence of zinc porphyrin on V_{OC} has mostly been attributed to the electron lifetime under illuminated open circuit voltage, which is related to several factors such as the molecular bonding orientations and the position of substituents.

EIS is a powerful technique for characterizing the important interfacial charge transfer and carrier transportation process in DSSCs. In order to realize the lifetime of electrons in TiO_2 under V_{OC} conditions, we measured the EIS of *cis*-2S2A and *trans*-2S2A under AM 1.5 solar illumination. Fig. 9 shows the

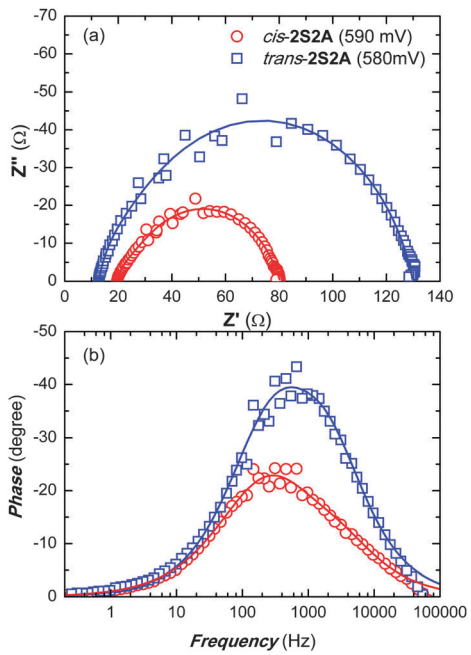

Fig. 9 (a) Nyquist plots and (b) Bode plots of *cis*-2S2A and *trans*-2S2A DSSCs under AM 1.5 G solar simulation light illumination and open circuit condition.

Table 4 Fitting results of Nyquist plots of *cis*-2S2A and *trans*-2S2A cells at *V*oc under AM 1.5 G illumination

Dye	R_{rec} (Ω)	CPE_{rec} (F)	τ_{rec} (ms)	τ_{pt} (ms)
cis-2S2A	56.3	1.28×10^{-4}	7.2	0.21
trans-2S2A	110.2	3.78×10^{-5}	4.2	0.20

Nyquist and Bode plots for DSSCs based on *cis*-2S2A and *trans*-2S2A under V_{OC} and AM 1.5 G illumination conditions. The EIS data were analyzed with equivalent circuit model consisting of dye-TiO_2/electrolyte interface and electrolyte/Pt-TCO interface with Z-view program. The analyzed results of EIS are summarized in Table 4 and indicate that the electron lifetime of 7.2 ms for *cis*-2S2A is longer than that of 4.2 ms for *trans*-2S2A, and the lifetimes of regeneration redox with Pt-TCO are about 0.2 ms for both *cis*-2S2A and *trans*-2S2A molecules.

The electron lifetime is related to the product of resistance of charge recombination (R_{rec}) and capacitance (CPE) between the TiO_2 and electrolyte interfaces. The longer electron lifetime of *cis*-2S2A is mostly attributed to the large CPE value, which means electron density in TiO_2 is higher for *cis*-2S2A under V_{OC} conditions. However, the EIS results reveal that the resistance of charge recombination of *cis*-2S2A (56.3 Ω) is smaller than that of *trans*-2S2A (110.2 Ω). The difference of charge recombination resistances for *cis*-2S2A and *trans*-2S2A is attributed to the orientation of dyes on TiO_2. The adsorbing molecules on TiO_2 can protect electrons from recombining with triiodide in the electrolyte near the interface. A larger size and a longer alkyl chain of dyes can increase the resistance of charge recombination. Therefore, the R_{rec} of *trans*-2S2A is larger than that of *cis*-2S2A as the distance between the surface of the TiO_2 and I_3^- close to the surface of *trans*-2S2A is longer because *trans*-2S2A is bound on the TiO_2 using a single carboxyphenyl group. Fig. 9(b) shows the Bode plots of DSSCs based on *cis*-2S2A and *trans*-2S2A under AM 1.5 G solar illumination conditions. The Bode phase plots of both *cis*-2S2A and *trans*-2S2A exhibits a broad single peak from 10 to 10 000 Hz. In general, the electron lifetime (τ_n) can be estimated from the frequency peak (f_p) as follows.[45,46]

$$\tau_n = \frac{1}{2\pi f_p}$$

The frequency peak of the DSSC based on *cis*-2S2A shifts to a lower frequency with respect to the DSSC based on *trans*-2S2A. The electron lifetimes under V_{OC} conditions estimated by Fig. 9(b) are 0.51 and 0.29 ms for *cis*-2S2A and *trans*-2S2A, respectively. The values of electron lifetime calculated from Bode plots are smaller than those calculated by fitting with equivalent circuits caused by the broadened peaks, which could be a combination of two frequency peaks from the charge recombination and charge transport from platinum.

EIS measurements under dark conditions

The electronic processes in DSSCs were well described by the transmission line model shown in Scheme 2. The equivalent

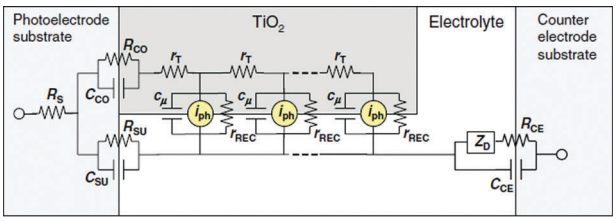

Scheme 2 Transmission line model of electronic processes in DSSCs.

circuit elements have the following meaning: R_S is the series resistance; R_{CO} and C_{CO} are charge transfer resistance and double layer capacitance at the T_{CO}/electrolyte interface, respectively; R_t and R_{rec} are electron transport through the TiO_2 nanoparticles and charge recombination resistance at the TiO_2/dye/electrolyte interface, respectively; and C_μ is the chemical capacitance of TiO_2.

Fig. 10(a) shows Nyquist plots of *cis*-2S2A and *trans*-2S2A sensitized solar cells with applied potential of 600 mV in dark conditions, and Fig. 10(b) shows the chemical capacitance of TiO_2 based on *cis*-2S2A and *trans*-2S2A as a function of applied potential in dark conditions. Based on the analysis of dark Nyquist plots with the transmission line model, the charge recombination resistance (690 Ω) of *cis*-2S2A is smaller than R_{rec} (929 Ω) of *trans*-2S2A. However, the chemical potential of *cis*-2S2A is larger than *trans*-2S2A under reversed applied voltage. The smaller R_{rec} indicates an inefficient molecular shielding of *cis*-2S2A, which might be attributed to the charge recombination in *cis*-2S2A, containing exposed thienyl groups. For *trans*-2S2A, the two thienyl substitutes are not as boldly exposed to the electrolyte due to its dense packing on the TiO_2 surface after adsorption giving higher recombination resistance. It is noticeable that Fig. 10(b) shows larger chemical capacitances for *cis*-2S2A/TiO_2 than that of *trans*-2S2A/TiO_2. It indicates that the electron densities of states of TiO_2 can be affected by the orientation of isomeric sensitizers on TiO_2. When *cis*-2S2A and *trans*-2S2A adsorb on the TiO_2 surface, the distance between electrolyte and TiO_2 surface for *trans*-2S2A is longer than *cis*-2S2A due to the different binding mode on TiO_2 surface. The steric hindrance due to the sensitized porphyrins on TiO_2 could inhibit lithium ions from reaching the surface of TiO_2, so the longer distance of *trans*-2S2A on TiO_2 might decrease the density of states of TiO_2, which increases the voltage on TiO_2 under the same amount of injected electrons. The population of densities of states (DOS) on TiO_2 is mainly influenced by the concentration of lithium ions on the surface, which interact with electrons on TiO_2, so the molecular orientation of *trans*-2S2A decreases the concentration of surface lithium ions.

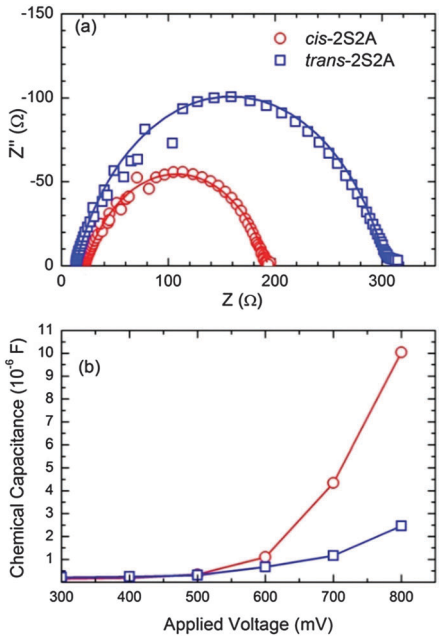

Fig. 10 (a) Nyquist plots for DSSCs with 600 mV applied voltage in dark conditions based on *cis*-2S2A and *trans*-2S2A. (b) Chemical capacitance of the TiO_2 of *cis*-2S2A and *trans*-2S2A as a function of applied bias potential from EIS measurements in dark conditions.

Conclusions

We report results from quantum chemical calculations, femtosecond fluorescence decay and electrochemical impedance spectroscopy measurements to rationalize the photovoltaic performances of devices fabricated using the *cis*- and *trans*-isomers of a model zinc porphyrin system. The DFT calculations revealed that in the LUMO of *cis*-2S2A, a small amount of electron density is localized over one carboxyphenyl group, whereas in case of the *trans*-2S2A there is no electron density on the anchoring carboxyphenyl. Due to the dual anchoring mode of the *cis* isomer, there is a chance of increased electron injection involving the LUMO orbital and higher excited states, whereas in the *trans* isomer, the electron injection is feasible only through the higher excited states. This observation is well supported by Mullikan charge analysis. From femtosecond fluorescence up-conversion measurements, we observed that the excited-state lifetime of *cis*-2S2A on Al_2O_3 is twice as long as that of *trans*-2S2A on Al_2O_3. Moreover, the electron injection time for *cis*-2S2A is longer than that for *trans*-2S2A. Electrochemical impedance measurements under one sun illumination also reveal that the charge recombination time of *cis*-2S2A is longer than that of *trans*-2S2A. Collectively, superior electron injection, longer excited-state lifetime, and higher electron injection yield are responsible for the photovoltaic performance of the *cis*-2S2A device being greater than that of its *trans*-2S2A counterpart. This thorough study will be an important guideline for the development of future dual anchoring porphyrin dyes for DSSCs.

Acknowledgements

Authors greatly acknowledge the financial supports from the Ministery of Science and Technology and Academia Sinica, Taiwan.

Notes and references

1 B. O'Regan and M. Grätzel, *Nature*, 1991, **353**, 737–740.
2 M. Gratzel, *Nature*, 2001, **414**, 338–344.
3 M. Grätzel, *Acc. Chem. Res.*, 2009, **42**, 1788–1798.
4 A. Hagfeldt, G. Boschloo, L. Sun, L. Kloo and H. Pettersson, *Chem. Rev.*, 2010, **110**, 6595–6663.
5 Y.-S. Yen, H.-H. Chou, Y.-C. Chen, C.-Y. Hsu and J. T. Lin, *J. Mater. Chem.*, 2012, **22**, 8734–8747.
6 L.-L. Li and E. W.-G. Diau, *Chem. Soc. Rev.*, 2013, **42**, 291–304.
7 H. Imahori, T. Umeyama and S. Ito, *Acc. Chem. Res.*, 2009, **42**, 1809–1818.
8 T. Higashino and H. Imahori, *Dalton Trans.*, 2015, **44**, 448–463.
9 Y. Tachibana, S. A. Haque, I. P. Mercer, J. R. Durrant and D. R. Klug, *J. Phys. Chem. B*, 2000, **104**, 1198–1205.
10 C.-L. Wang, C.-M. Lan, S.-H. Hong, Y.-F. Wang, T.-Y. Pan, C.-W. Chang, H.-H. Kuo, M.-Y. Kuo, E. W.-G. Diau and C.-Y. Lin, *Energy Environ. Sci.*, 2012, **5**, 6933–6940.
11 C.-L. Wang, J.-Y. Hu, C.-H. Wu, H.-H. Kuo, Y.-C. Chang, Z.-J. Lan, H.-P. Wu, E. Wei-Guang Diau and C.-Y. Lin, *Energy Environ. Sci.*, 2014, **7**, 1392–1396.
12 C.-H. Wu, M.-C. Chen, P.-C. Su, H.-H. Kuo, C.-L. Wang, C.-Y. Lu, C.-H. Tsai, C.-C. Wu and C.-Y. Lin, *J. Mater. Chem. A*, 2014, **2**, 991–999.
13 J.-W. Shiu, Y.-C. Chang, C.-Y. Chan, H.-P. Wu, H.-Y. Hsu, C.-L. Wang, C.-Y. Lin and E. W.-G. Diau, *J. Mater. Chem. A*, 2015, **3**, 1417–1420.
14 T. Bessho, S. M. Zakeeruddin, C.-Y. Yeh, E. W.-G. Diau and M. Grätzel, *Angew. Chem., Int. Ed.*, 2010, **49**, 6646–6649.
15 A. Yella, H.-W. Lee, H. N. Tsao, C. Yi, A. K. Chandiran, M. K. Nazeeruddin, E. W.-G. Diau, C.-Y. Yeh, S. M. Zakeeruddin and M. Grätzel, *Science*, 2011, **334**, 629–634.
16 A. Yella, C.-L. Mai, S. M. Zakeeruddin, S.-N. Chang, C.-H. Hsieh, C.-Y. Yeh and M. Grätzel, *Angew. Chem., Int. Ed.*, 2014, **53**, 2973–2977.
17 S. Mathew, A. Yella, P. Gao, R. Humphry-Baker, F. E. CurchodBasile, N. Ashari-Astani, I. Tavernelli, U. Rothlisberger, K. NazeeruddinMd and M. Grätzel, *Nat. Chem.*, 2014, **6**, 242–247.
18 M. K. Nazeeruddin, R. Humphry-Baker, D. L. Officer, W. M. Campbell, A. K. Burrell and M. Grätzel, *Langmuir*, 2004, **20**, 6514–6517.
19 F. Odobel, E. Blart, M. Lagree, M. Villieras, H. Boujtita, N. El Murr, S. Caramori and C. Alberto Bignozzi, *J. Mater. Chem.*, 2003, **13**, 502–510.
20 C. Y. Lee, C. She, N. C. Jeong and J. T. Hupp, *Chem. Commun.*, 2010, **46**, 6090–6092.
21 M. K. Panda, G. D. Sharma, K. R. Justin Thomas and A. G. Coutsolelos, *J. Mater. Chem.*, 2012, **22**, 8092–8102.
22 H. Imahori, Y. Matsubara, H. Iijima, T. Umeyama, Y. Matano, S. Ito, M. Niemi, N. V. Tkachenko and H. Lemmetyinen, *J. Phys. Chem. C*, 2010, **114**, 10656–10665.
23 T. Higashino, Y. Fujimori, K. Sugiura, Y. Tsuji, S. Ito and H. Imahori, *J. Porphyrins Phthalocyanines*, 2015, **19**, 140–149.
24 D. Daphnomili, G. Landrou, S. Prakash Singh, A. Thomas, K. Yesudas, K. Bhanuprakash, G. D. Sharma and A. G. Coutsolelos, *RSC Adv.*, 2012, **2**, 12899–12908.
25 J. Lu, X. Xu, Z. Li, K. Cao, J. Cui, Y. Zhang, Y. Shen, Y. Li, J. Zhu, S. Dai, W. Chen, Y. Cheng and M. Wang, *Chem. – Asian J.*, 2013, **8**, 956–962.
26 E. C.-H. Kwok, M.-Y. Chan, K. M.-C. Wong and V. W.-W. Yam, *Chem. – Eur. J.*, 2014, **20**, 3142–3153.
27 R. Ambre, K.-B. Chen, C.-F. Yao, L. Luo, E. W.-G. Diau and C.-H. Hung, *J. Phys. Chem. C*, 2012, **116**, 11907–11916.
28 R. B. Ambre, G.-F. Chang, M. R. Zanwar, C.-F. Yao, E. W.-G. Diau and C.-H. Hung, *Chem. – Asian J.*, 2013, **8**, 2144–2153.
29 R. B. Ambre, G.-F. Chang and C.-H. Hung, *Chem. Commun.*, 2014, **50**, 725–727.
30 R. B. Ambre, S. B. Mane, G.-F. Chang and C.-H. Hung, *ACS Appl. Mater. Interfaces*, 2015, **7**, 1879–1891.
31 S. B. Mane, L. Luo, H.-H. Tsai and C.-H. Hung, *J. Porphyrins Phthalocyanines*, 2015, **19**, 695–707.
32 S. B. Mane and C.-H. Hung, *New J. Chem.*, 2014, **38**, 3960–3972.
33 S. B. Mane, L. Luo, G.-F. Chang, E. W.-G. Diau and C.-H. Hung, *J. Chin. Chem. Soc.*, 2014, **61**, 545–555.
34 S. B. Mane, J.-Y. Hu, Y.-C. Chang, L. Luo, E. W.-G. Diau and C.-H. Hung, *Chem. Commun.*, 2013, **49**, 6882–6884.
35 S. B. Mane and C.-H. Hung, *Chem. – Eur. J.*, 2015, **21**, 4825–4841.
36 M. J. Frisch, G. W. Trucks, H. B. Schlegel, G. E. Scuseria, M. A. Robb, J. R. Cheeseman, G. Scalmani, V. Barone, B. Mennucci, G. A. Petersson, H. Nakatsuji, M. Caricato, X. Li, H. P. Hratchian, A. F. Izmaylov, J. Bloino, G. Zheng, J. L. Sonnenberg, M. Hada, M. Ehara, K. Toyota, R. Fukuda, J. Hasegawa, M. Ishida, T. Nakajima, Y. Honda, O. Kitao, H. Nakai, T. Vreven, J. A. Montgomery Jr., J. E. Peralta, F. Ogliaro, M. J. Bearpark, J. Heyd, E. N. Brothers, K. N. Kudin, V. N. Staroverov, R. Kobayashi, J. Normand, K. Raghavachari, A. P. Rendell, J. C. Burant, S. S. Iyengar, J. Tomasi, M. Cossi, N. Rega, N. J. Millam, M. Klene, J. E. Knox, J. B. Cross, V. Bakken, C. Adamo, J. Jaramillo, R. Gomperts, R. E. Stratmann, O. Yazyev, A. J. Austin, R. Cammi, C. Pomelli, J. W. Ochterski, R. L. Martin, K. Morokuma, V. G. Zakrzewski, G. A. Voth, P. Salvador, J. J. Dannenberg, S. Dapprich, A. D. Daniels, Ö. Farkas, J. B. Foresman, J. V. Ortiz, J. Cioslowski and D. J. Fox, *Gaussian 09*, Gaussian, Inc., Wallingford, CT, USA, 2009.
37 N. Papageorgiou, W. F. Maier and M. Gratzel, *J. Electrochem. Soc.*, 1997, **144**, 876–884.
38 C.-P. Hsieh, H.-P. Lu, C.-L. Chiu, C.-W. Lee, S.-H. Chuang, C.-L. Mai, W.-N. Yen, S.-J. Hsu, E. W.-G. Diau and C.-Y. Yeh, *J. Mater. Chem.*, 2010, **20**, 1127–1134.
39 C.-Y. Lin, C.-F. Lo, L. Luo, H.-P. Lu, C.-S. Hung and E. W.-G. Diau, *J. Phys. Chem. C*, 2009, **113**, 755–764.
40 K. Shankar, J. Bandara, M. Paulose, H. Wietasch, O. K. Varghese, G. K. Mor, T. J. LaTempa, M. Thelakkat and C. A. Grimes, *Nano Lett.*, 2008, **8**, 1654–1659.

41 L. Luo, C.-F. Lo, C.-Y. Lin, I. J. Chang and E. W.-G. Diau, *J. Phys. Chem. B*, 2006, **110**, 410–419.
42 H.-P. Lu, C.-Y. Tsai, W.-N. Yen, C.-P. Hsieh, C.-W. Lee, C.-Y. Yeh and E. W.-G. Diau, *J. Phys. Chem. C*, 2009, **113**, 20990–20997.
43 A. Usami, S. Seki, Y. Mita, H. Kobayashi, H. Miyashiro and N. Terada, *Sol. Energy Mater. Sol. Cells*, 2009, **93**, 840–842.
44 T. Marinado, K. Nonomura, J. Nissfolk, M. K. Karlsson, D. P. Hagberg, L. Sun, S. Mori and A. Hagfeldt, *Langmuir*, 2010, **26**, 2592–2598.
45 R. Kern, R. Sastrawan, J. Ferber, R. Stangl and J. Luther, *Electrochim. Acta*, 2002, **47**, 4213–4225.
46 J. A. Mikroyannidis, P. Suresh, M. S. Roy and G. D. Sharma, *Electrochim. Acta*, 2011, **56**, 5616–5623.